Design of high-speed synchronous reluctance machines

Design of High-Speed Synchronous Reluctance Machines

Francesco Cupertino, Marco Palmieri
Dept. of Electrical Engineering and Information Technology
Politecnico di Bari
Bari, Italy
francesco.cupertino@poliba.it

Gianmario Pellegrino
Dept. of Energy
Politecnico di Torino
Torino, Italy
gianmario.pellegrino@polito.it

***Abstract*— This paper considers the electromagnetic and structural co-design of synchronous reluctance (SyR) machines for high-speed applications, with the aid of optimization algorithms. The aim of this work is twofold. First, three commercial electrical steel grades are compared to establish quantitatively how steel properties influence the performance of high-speed SyR machines. The considered steel grades are two cobalt-iron alloys and a high-grade non-oriented silicon steel. Second, an original design method is proposed, targeting maximum power density. The results of the analysis show that for the considered machine output power grows with rotational speed up to 70 krpm. Over such speed limit, the performance degrades due to structural limitations. The proposed design procedure is implemented using open source software.**

Keywords — AC machines; High-speed electrical machines; Design Optimization; Synchronous reluctance machines; Finite Element Analysis; Design automation;

I. INTRODUCTION

In several application areas, there is a growing interest in high-speed electrical machines [1], because they allow compactness and reliability. For example, direct-drive high-speed actuators permit to eliminate the need for a mechanical gearbox, reducing the system weight and increasing its efficiency [2]. As the rotational speed of the electrical machine grows, structural integrity of the rotor tends to become a critical issue. [2]. Moreover, core loss quickly grows with the electrical frequency that is proportional to mechanical speed, resulting in augmented thermal stress. Rotor loss is particularly critical, because heat removal from the rotor would need special cooling systems, such as a hollow shaft with fluid circulation. Among the variety of high-speed brushless machines, Permanent Magnet (PM) synchronous machines exhibit the highest torque density but also the highest cost, due to rare heart PMs, and the worse collateral effects in case of fault: high voltage at open circuit uncontrolled conditions and high braking torque in short-circuit conditions. Moreover, a retaining sleeve is mandatory in surface PM machines, to withstand centrifugal stress and ensure rotor integrity [4], [5]. Unfortunately, retaining systems make rotor construction more complicated and can increase rotational loss.

Among the machines with no PMs, solid rotor induction machines are inherently robust, structural wise, but they have lower torque density and efficiency with respect to PM synchronous machines.

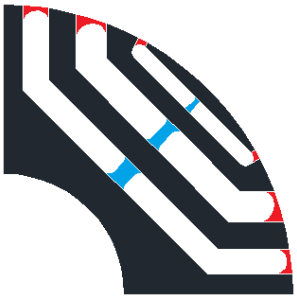

Fig. 1 – Sketch of a SyRM rotor with tangential (red) and radial (blue) ribs

Synchronous Reluctance (SyR) machines constitute a viable alternative to induction motors for industrial low speed applications [6]. They are easy to manufacture, and make use of standard processes and materials. Moreover, they are safe against converter faults due to the absence of magnets, and their excitation field can be adjusted so to limit iron loss when at partial load. The use of SyR machines in high-speed applications is usually discouraged because of their unsatisfactory structural properties. The rotor is kept together by tiny structural ribs, highlighted in Fig.1. If such ribs are thickened for the sake of rotor integrity at high speed, this tends to compromise the reluctance torque and then the performance: the thicker the ribs are, the lower reluctance torque and power factor will be.

This work considers the design of multiple barriers SyR machines for aerospace application. Reference is made to a generic aerospace actuator. The paper aims at finding the physical limits of speed scalability, and at assessing the limits of power density, accordingly. The first part of the paper investigates the aspect of electrical laminations choice. Two cobalt-iron alloys with very high magnetic saturation levels and different mechanical strength and a high-grade silicon steel with low losses and high yield strength are compared. Several SyR machines with same rated torque and outer envelope are designed and compared. The machines are designed with the aid of optimization algorithms focusing on cost functions of electromagnetic nature: torque and torque ripple. The size of the structural ribs is on line adjusted during the magnetic optimization according to a simplified structural model. The results of the analysis demonstrate that using cobalt-iron is convenient at relatively low speed ratings (below 20000 rpm), and that the advantage of cobalt-iron of permitting a flux density over 2 Tesla progressively vanishes with the increase of the

speed rating, due to iron loss. This result is valid for both the considered types of cobalt-iron.

In the second part of the paper, an original procedure to determine the maximum output power achievable from a given active volume is presented. Also in this case, optimization algorithms are adopted at the design stage. The objective functions this time are output power and torque ripple. Rotational speed is an optimization input. Normally, if speed increases, power is bound to increase. However, ribs width also grows with speed, and the algorithm finds a trade-off between the two aspects. Given the stack volume and electric loading, the algorithm optimizes the machine geometry and the rated speed so to determine the maximum feasible power and therefore the speed limit: if speed increases further, output power would decrease. The design procedure is repeated through a range of values of thermal loading, to take into account the effects of thermal aspects towards power density and obtainable output power. Effects of changing the stack volume and adding permanent magnets to improve torque and power factor are also investigated in the paper.

II. Problem Statement

The stator and rotor geometries are defined in Fig.2. In the first part of the paper, the comparison among different lamination material is carried out considering a target torque of 1.6 Nm to be developed within a volume equal to 0.25 dm^3 for active parts. Several designs have been executed considering different rated speeds in the range 5 - 50 krpm. Consequently, rated power was in the range 0.8 - 8 kW, because all the machines have the same rated torque. Table I reports the common machine specifications that will remain unchanged throughout the entire paper.

A. Lamination Materials

The lamination parameters most affecting the performances of high-speed machines are the saturation flux density the iron losses and the material Yield strength

TABLE I - MACHINE SPECIFICATIONS

Parameter	Value	Units
Stator outer diameter	80	mm
Axial length	50	mm
Airgap	0.25	mm
Pole pairs	2	--
Stator slots	24	--
Slot filling factor	0.4	--
Torque ripple	< 10	%

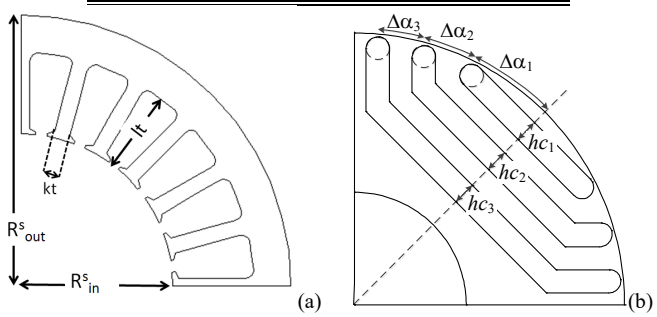

Fig. 2 – Parameterization of stator (a) and rotor (b) laminations.

To determine the most suitable lamination material to realize high-speed synchronous reluctance machines, two cobalt-iron (CoFe) and one silicon-iron (SiFe) alloys are considered. Each material excels in one of the features mentioned above (flux density, losses, strength). The main lamination properties are summarized in Table II. The two CoFe machines share the same stator lamination material thermally treated for maximizing its magnetic properties (Vacodur49 "opt. mag."). Vacodur49 is produced by Vacuumschmelze [7] and will be referred to as V_49 in the following. The rotor of the first CoFe machine is made of V_49 "opt. mec.", where the thermal treatment is the one for maximum mechanical strength. This is obtained at the expenses of magnetic properties. The rotor of the second CoFe machine is made of Vacodur S plus (hereinafter referred to as V_S+). V_49 "opt. mec." and V_S+ have yield strengths equal to 390 MPa and 750 MPa respectively, but the latter material has higher core losses. The last grade under comparison is the SiFe alloy 10JNEX900 (hereinafter referred to as J_900) produced by JFE Steel Corporation [8] with a lamination thickness of 0.1 mm, a lower saturation flux density (less than 1.5 T), yield strength around 600 MPa and reduced core losses. The third design has both stator and rotor made of J_900. Fig.3 shows the BH curves for the aforementioned materials.

TABLE II – PROPERTIES OF THE IRON ALLOYS

Lamination Type	V_49 opt-mag	V_49 opt-mec	V_S+	J_900
Loss @ 50 Hz, 1.5 T [W/kg]	1.27	2.78	13.51	1.46*
Loss @ 400 Hz, 1.5 T [W/kg]	14.7	26.4	122.1	14.8*
Yield strength [MPa]	210	390	750	604
Mass density [kg/m^3]	8120	8120	8120	7490

* Extrapolated values

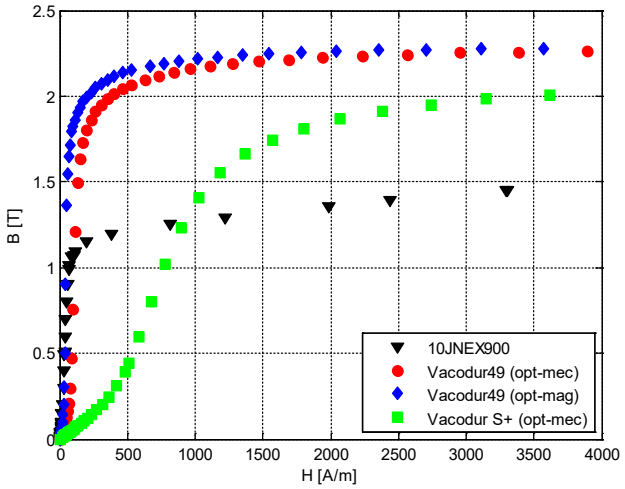

Fig. 3 – BH characteristics of the considered lamination materials

B. Motor Parameterization

Stator and rotor geometries have been defined with the aid of optimization algorithms and FEMM simulations using SyR-e open source platform [9]. All the considered machines have 24 stator slots and three rotor flux barriers per pole. These numbers have been extensively recognized by the related literature as one of the good stator - rotor combinations in terms of average torque to torque ripple tradeoff [10]. The stator parameters designed by the optimization algorithm are: the tooth length l_t and width w_t and the machine split ratio SR, defined as the ratio between stator inner and outer diameters. The above mentioned parameters are defined in Fig.2a. Dealing with the rotor, the automatically designed parameters are the barriers widths hc_i and their positions at the airgap $\Delta\alpha_i$, shown in Fig.2b. The tangential iron ribs (the ones at the flux barriers ends) are fixed and chosen according to mechanical tolerances of cutting process. Where needed, inner posts are automatically added during the optimization, as described in subsection II.C. The final machine designs are verified by means of static structural FEA. It is then assumed that the radial ribs are responsible for the structural integrity at high-speed regimes while tangential ribs are kept to minimum thickness within the limits of the cutting process.

C. Autmatic Calculation of Radial Ribs Thickness

For each rotor candidate, the radial ribs' thicknesses are automatically calculated according to a simple analytical model. For example, the j-th radial rib supports the centrifugal stress of the total external iron region (blue area) represented in Fig.4. The j-th centrifugal force F_j corresponding to the iron mass M_j of the blue region is evaluated considering that the mass is concentrated in its center of gravity G_j:

$$F_j = \mathrm{M_j} \cdot r_j \cdot \omega_{max}^2 \tag{1}$$

where r_j is the radius of the j-th center of gravity and ω_{max} is the maximum rotational speed. Given the centrifugal forces, the width w_{rj} of the j-th radial rib is calculated according to the material yield strength σ_{max}:

$$w_{rj} = \frac{F_j}{(L \cdot k_{sf} \cdot \sigma_{max})} \tag{2}$$

where k_{sf} is the safety factor, selected to 1 in the following. The rib size (2) is calculated for each barrier. When w_{rj} results lower than the manufacturing tolerance, the corresponding radial rib is not included in the rotor geometry. At the end of optimization the rotor geometry is verified with FEA-based centrifugal test. If needed, a radial rib having thickness equal to the manufacturing tolerance is added to the barriers without ribs. For high speed machines, it could happen that the structural FEA evidences a maximum stress located in the tangential ribs and this value could be above the maximum allowed stress. In the designs considered here it was always possible to reduce the maximum stress values by splitting in two equal parts the radial ribs and moving them closer to the tangential ribs. This reduces the flux guide deformation and, consequently, the stress in the tangential ribs. Another effective change is to rotate the split ribs towards the centre of the pole at the airgap. The split, move and rotate procedure was optimized by trial and error until the maximum stress fell below the chosen limit.

III. Comparison of Alloys Performance

In order to compare the different core materials, a common torque target was fixed and the stator current was consequently adjusted. Several optimization runs were executed at three rated speed levels and equal target torque. Speed values are 5 krpm, 25 krpm and 50 krpm. The objectives of the optimization were the average torque and torque ripple, following the approach described in [11]. Hereinafter, for sake of simplicity, optimized machines will be identified by acronyms reminding the respective rotor material ("V" for Vacodur49, "VS" for Vacodur S plus and "J" for 10JNEX900) and a number which indicates the rated speed expressed in krpm. For example, the optimized laminations shown in the first column of Fig.5 refer to 50 krpm and are indicated as V50 (a), VS50 (b) and J50 (c), respectively.

A. Optimal Geometries

All J-type machines have ticker back-iron due to the lower saturation level of SiFe steel 10JNEX900 with respect to CoFe. VS- and J-types rotors have smaller radial and tangential ribs respect to V-type ones, due to the higher yield strength of the respective materials. The second column of Fig.5 reports the results of the centrifugal test to check rotor feasibility after structural optimization. As described before, the split, move and rotate procedure was applied to the radial ribs to limit maximum stress.

B. Power Factor, Losses and Efficiency

Fig.6 compares the power factors (PF) of all materials and all considered speeds. At high speed the power factor deteriorates due to the ticker structural ribs that allow larger q-axis flux diminishing machine saliency. At high speed (e.g. 50 krpm), the J-series and VS-series machines exhibit better PF values than V-series ones. The adoption of very high saturation alloy with poor structural properties produces two effects: firstly a thicker iron post is required to withstand centrifugal stress, secondly the ribs saturate at higher flux density. Both causes contribute to worsen power factor. Fig.7 and Fig.8 report the detail of iron and copper losses and efficiency. It is clear that, at relatively low speeds (5000 rpm), the better saturation flux density allow the machines with Vacodur49 to reach higher efficiency values

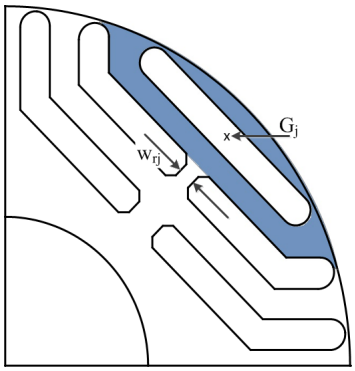

Fig. 4 – Definition of the inner post geometry

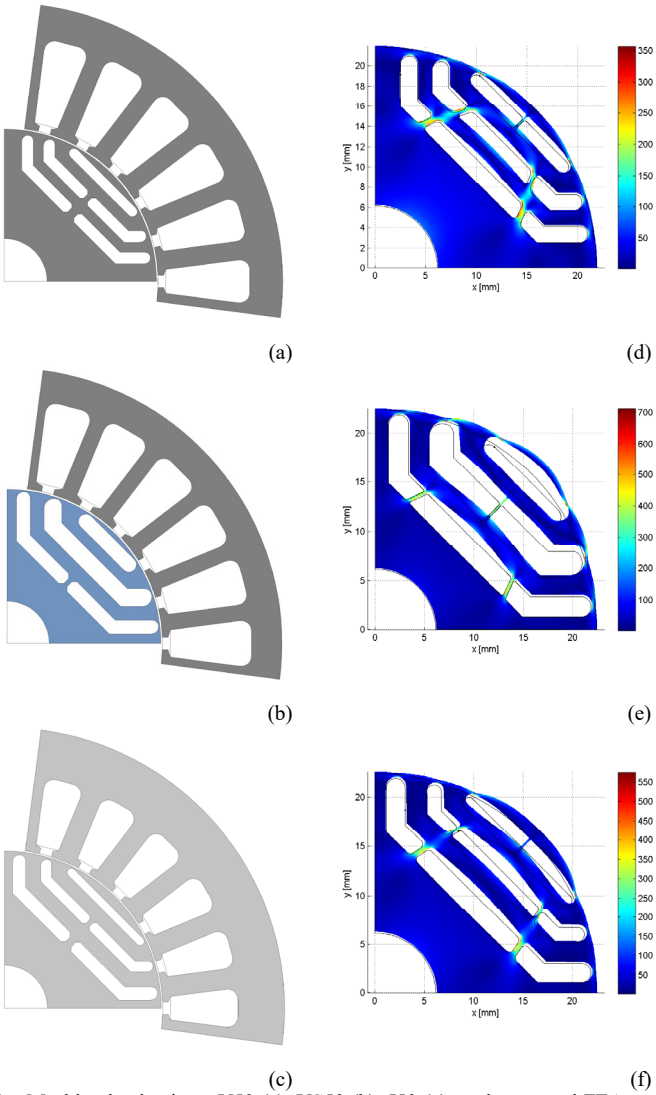

Fig. 5 – Machine laminations: V50 (a), VS50 (b), J50 (c) and structural FEA analysis of 50krpm machines with refined radial posts: $V50_{mod}$ (d), $VS50_{mod}$ (e), $J50_{mod}$ (f)

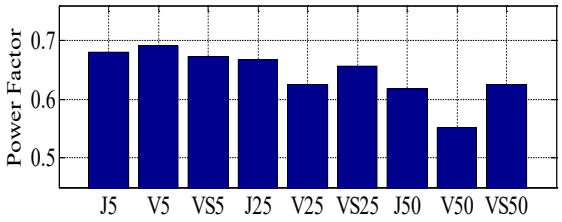

Fig. 6 – Power Factor of V-series, VS-series and J-series machines at 5krpm, 25 krpm and 50krpm

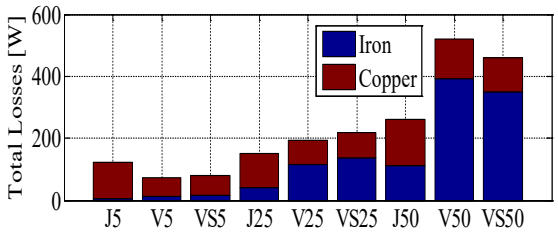

Fig. 7 – Loss distribution [W] of V-series, VS-series and J-series machines at 5krpm, 25 krpm and 50krpm

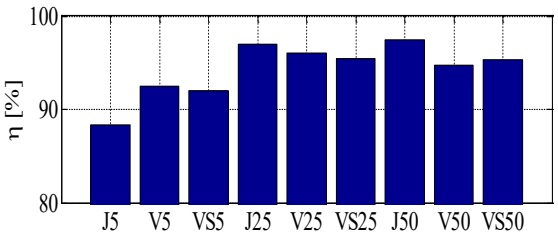

Fig. 8 – Efficiency [%] of V-series, VS-series and J-series machines at 5krpm, 25 krpm and 50krpm

The J- machines require a greater current level to give the same target torque. This causes higher copper losses for the same output power. At low speeds iron losses are negligible, so the efficiency of the V5-machine is higher than the one of the J5 competitor. Above 25 krpm this trend is reversed, because the main factors influencing the power capability become maximum stress in the rotor and, above all, losses. At high rotational speeds, iron to copper losses ratio increases and J-series motors become more efficient despite of the higher Joule losses. Finally, J- and VS- machines maintain reasonable power factor values also at 50 krpm. In conclusion, as evidenced also in [12], above a certain speed (and fundamental frequency) limiting iron losses is crucial to improve machine performances. Material with lower magnetic properties but also reduced losses such as SiFe with high silicon content or ferrites may become a feasible choice in high-speed applications.

IV. Maximization of Power Density

Having identified the 10JNEX900 as the most promising material for high-speed SyR machines among the considered alloys, this section presents a method to determine maximum feasible speed maximizing power density, given structural and thermal constrains. High-speed machines are a common choice to increase power over volume density in electrical machines. The limits to the increase of speed are centrifugal forces, iron losses, additional copper losses and critical speeds of the rotor [3], [12], [12]. In this work, we neglect the last two phenomena in the design stage, assuming that the rotor is short and rigid enough not to experience important resonances and windings are realized so to minimize skin effect and proximity losses [12]. Note that a final verification of this assumption is always needed before manufacturing. In this section, the attention is focused on rotor design and definition of the base speed to improve power density. Output power and torque ripple are optimized here, intended that rated speed is optimized by the design algorithm to

find maximum power in consideration of thermal and structural limits.

A. Procedure

In the following optimization procedure, the stator geometry is kept unchanged, with a split ratio SR equal to 0.59 derived from the previous optimization stage. This choice was made to simplify the calculation of iron losses but, in principle, the procedure could be applied to the contemporaneous optimization of both stator and rotor geometries. As said, admissible losses are a key factor, determined mainly by the cooling system. It is assumed that the heat produced by the losses will be exchanged using the stator external surface using air or liquid cooling systems. The coefficient k_j is defined as the ratio of admitted total losses divided by the stator external surface. Typical values are 3 kW/m^2 for natural cooled machines, 10 kW/m^2 for forced ventilation and up to 40 kW/m^2 with liquid cooling and end windings potting. Total admissible losses are then defined as (3):

$$P_{TOT} = k_j \pi D L \tag{3}$$

where D and L are the outer diameter and the axial length of the machine stator core. Rotor core losses are neglected during machine design and post evaluated off-line. Stator iron losses (P_{FeS}) are included in the optimization. Since the stator geometry is given, iron losses were calculated using FEA software at a single speed value and then adapted to different speed levels using Steinmetz equation. Therefore, the admissible current amplitude I_n for each candidate machine is:

$$I_n = \sqrt{\frac{P_{TOT} - P_{FeS}(\omega)}{3 \cdot R_S}} \tag{4}$$

where R_s is the phase resistance. The mechanical base speed is included among the parameters to be selected by the optimization algorithm, together with the rotor geometry and current phase angle γ [11]. Output torque is FEA calculated and the output power follows as the product of mechanical speed and average torque. Output power and torque ripple are used as objectives for the multi-objective optimization algorithm. The optimization procedure is similar to the one described in the previous section. For each rotor design, the thickness of radial ribs is calculated considering iron mass and mechanical speed which is now different for each candidate machine. To maximize output power the optimization algorithm tentatively increases the speed, but this also increases P_{FeS} and the thickness of the structural ribs. Therefore a tradeoff speed is finally found, leading to maximum power. Over this speed, output power does not increase anymore due to available current reduction (4) and excessive ribs size. This speed will be automatically found by the optimization algorithm. Torque ripple optimization avoids final designs with high output power but very poor torque quality, which is not unlikely with SyR machines. We are aware that the exclusion of stator parameters from the optimization could led to suboptimal solutions, but this does not diminish the contribution of the paper. The proposed procedure could be easily repeated considering different split ratios or slot/teeth thickness ratio to determine the most suitable stator configuration for power density maximization. As mentioned before, the bottleneck of the method is the calculation of iron losses that requires the knowledge of stator current. The latter is calculated in (4) assuming stator losses known. We are currently studying alternative approaches that may solve this problem using iterative procedures with minimal computational effort. Results considering stator and rotor joint optimization will be included in future publications.

B. Maximum Power Solutions

Several optimization runs have been performed for different k_j values, from 3 to 96 kW/m^2. Fig.9 reports the mechanical speed that maximizes output power as a function of admitted loss factor k_j. Figs. 10 and 11 report the charts of machine efficiency and power per volume density as a function of k_j, for the same optimal machines considered in Fig. 9.

Since the optimization algorithm maximizes the output power, it is worth noticing that the reported machines represent maximum power density limit, given the k_j value (Fig. 11). Power density grows with admitted loss. Maximum mechanical speed, instead, shows a plateau around 70 krpm (Fig. 9), in the area of k_j equal to 40 to 50 kW/m^2. Power density in that area is around 80 kW/dm^3 and the rotor tip speed is about 170 m/s.

Values of k_j greater than 50 kW/m^2 are not of practical interest but are reported to show that feasible speed tends to saturate. For the considered rotor diameter, above 70 krpm, the increase of iron losses and ribs thickness are challenging obstacles. Table III shows the losses distribution for the considered k_j values. Losses are well balanced between iron and copper for feasible k_j values (i.e. up to 45 kW/m^2).

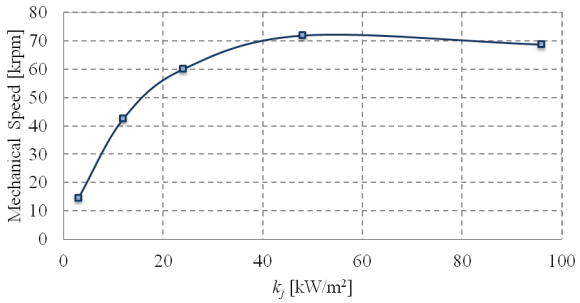

Fig. 9. Rotational speed for maximum output power, as a function of loss factor k_j.

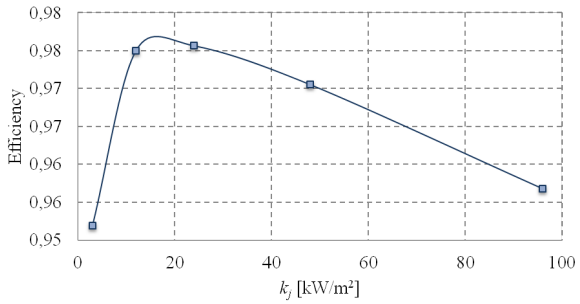

Fig. 10. Efficiency, as a function of k_j (stator loss only).

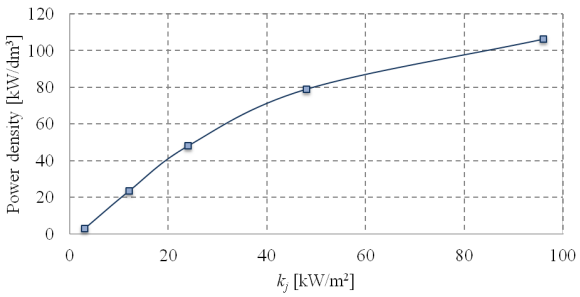

Fig. 11. Power density per volume, as a function of k_j.

TABLE III – DISTRIBUTION OF STATOR LOSSES BETWEEN IRON AND COPPER FOR SEVERAL k_j VALUES

	K_J = 3 [kW/m²]	K_J = 12 [kW/m²]	K_J = 24 [kW/m²]	K_J = 48 [kW/m²]	K_J = 96 [kW/m²]
Copper losses [W]	24	73	175	489	1194
Iron losses [W]	25	123	217	295	273
Total losses [W]	49	196	392	784	1467

Fig.12 shows stator and rotor laminations of the machine, hereinafter referred as *M1*, selected from the optimization run performed for k_j=24 kW/m². This machine represents a good compromise between feasibility (using liquid cooling system) efficiency and power density. One of the mayor drawbacks is its power factor, close to 0.5.

C. *Permanent Magnet Assistance*

Permanent magnets (PMs) inserted into the rotor flux barriers can increase both power factor and power density. The inclusion of the additional PM mass implies the recalculation of the radial ribs thickness including the PM mass in M_j in equation (1). This was done for *M1* machine considering NdFeB magnets N28EH from Arnold Magnetics having 1.085 T residual flux density and 200 °C maximum operating temperature. Different magnet quantities were included into the rotor, so to fill a certain percentage of the flux barrier. Situations going from 0% (no magnets) to 60% are documented in Table IV. Such magnet quantities can be easily inserted utilizing only the straight central segments of each rotor flux barrier. Power factor and output power values are reported in Table IV.

The drawing of machine *M1* with 40% of magnets (N28EH) is reported in Fig.13 to clarify where and how the PMs have been inserted, and to show the increased thickness of radial ribs, with respect to Fig. 12. The increase of radial ribs thickness due to the added mass is largely compensated by the PM flux both in terms of power factor and power density. The power factor increases up to 0.69 with just a 20% of PMs and approaches almost unity when the 60% of flux barriers are filled with PMs. Power density can increase by 60% in the considered PM assistance range.

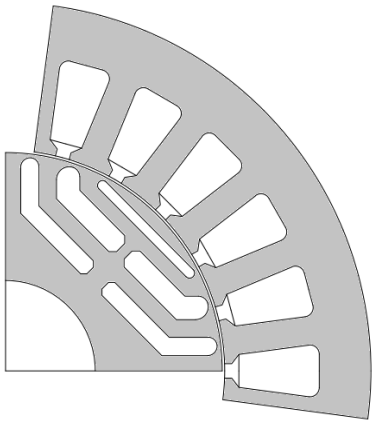

Fig. 12 – Cross section of M1 selected for k_i = 24 kW/m²

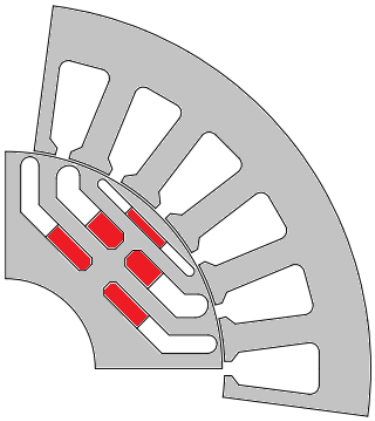

Fig. 13 – Cross section of M1 when 40% of each flux barrier is filled with PMs (evidenced in red)

V. STACK SIZE SCALABILITY

The procedure illustrated in Section IV was extended to machines with different volumes in order to point out some usefull scalability rules. Several power and torque ripple optimization runs were performed considering machines with the volume scaled by two times (*M2*) and ten times (*M10*) respect to machine *M1*. The aspect ratio (ratio between stator diameter and axial length) is the same of the baseline machine *M1*.

As volume increases the rotor radius grows up causing an increment of torque density (Fig.15) but also a reduction of maximum speed (Fig.14) due to the ticker radial ribs needed to withstand centrifugal forces. Since the maximum speed reduction is more pronounced than the torque increase, the power density reduces when specific losses (k_j) are kept constant (Fig. 16).

Also the machines with larger volumes suffer from a poor power factor, lower than 0.5 when k_j equals 24 kW/m². Table IV summarize the potential improvement obtainable with the insertion of PMs also in volume scaled machines. Similarly to the case of *M1* machine, the power factor increases about 90% in the considered PM range. The impact of PMs on power density is even more pronounced with larger machines that allow an increased airgap flux density and a better utilization of the rotor and stator core material.

TABLE IV – PERFORMANCE IMPROVEMENTS OBTAINED WITH THE INSERTION OF PMS

Percentage of flux barrier volume filled with PMs	*M1* PF [p.u.]	*M1* power [kW]	*M2* PF [p.u.]	*M2* power [kW]	*M10* PF [p.u.]	*M10* power [kW]
0% (no PMs)	0.51	15	0.49	30	0.40	116
20%	0.69	20	0.64	38	0.53	153
40%	0.85	23	0.8	45	0.65	183
60%	0.96	25	0.92	50	0.77	209

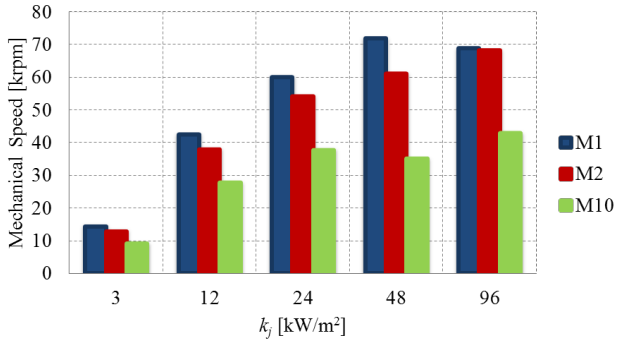

Fig. 14 – Maximum speed versus k_j values for different machine volumes

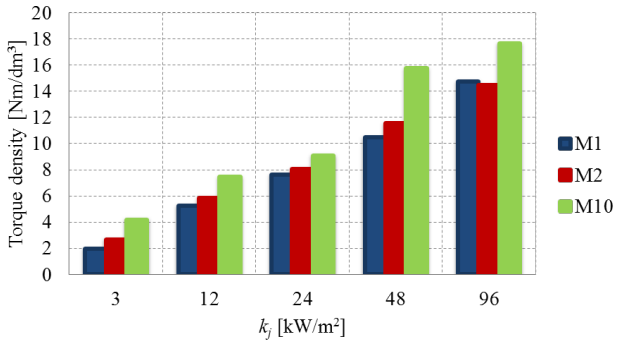

Fig. 15 – Torque density versus k_j values for different machine volumes

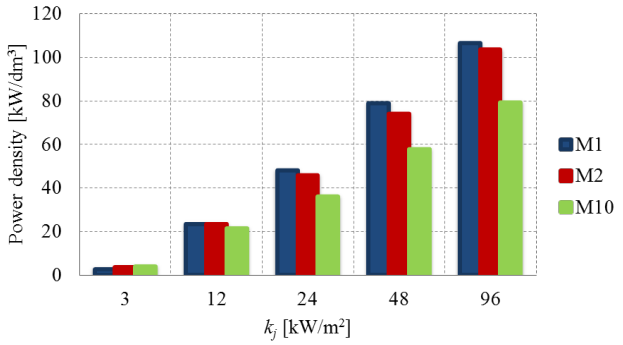

Fig. 16 – Power density versus k_j values for different machine volumes

VI. CONCLUSIONS

This paper considered the design of high-speed multi-barrier SyR machines. The investigation is focused on machines without retaining systems, where structural ribs ensure the rotor integrity towards centrifugal stress. The main contributions of the paper are 1) a comparison among commercial CoFe and SiFe alloys for the specific application and 2) a procedure to determine the speed and power density limits of SyR machines, given the stack size. It is demonstrated that limiting core losses is the most critical point in the design of high speed SyR machines. Moreover, given a stack size, there is a maximum rotational speed over which no further improvement of power density is obtained. The main limit of high-speed SyR machines is the poor power factor that could be improved with the insertion of PMs in the flux barriers. This procedure was described and the potential advantages in terms of power factor and power density were quantified.

REFERENCES

[1] Rahman, M.A.; Chiba, A.; Fukao, T., "Super high speed electrical machines - summary," Power Engineering Society General Meeting, 2004. IEEE , vol., no., pp.1272,1275 Vol.2, 10-10 June 2004.

[2] D. Gerada, A. Mebarki, N.L. Brown, C. Gerada, A. Cavagnino, A. Boglietti, "High-Speed Electrical Machines: Technologies, Trends, and Developments", IEEE Transactions on Industrial Electronics, Vol. 61, n. 6, 2014, pp. 2946-2959.

[3] Borisavljevic, A.; Polinder, H.; Ferreira, J.A., "On the Speed Limits of Permanent-Magnet Machines," Industrial Electronics, IEEE Transactions on , vol.57, no.1, pp.220,227, Jan. 2010.

[4] Binder, A.; Schneider, T.; Klohr, M., "Fixation of buried and surface-mounted magnets in high-speed permanent-magnet synchronous machines," Industry Applications, IEEE Transactions on , vol.42, no.4, pp.1031,1037, July-Aug. 2006.

[5] Krahenbuhl D., Zwyssig C., Weser H., Kolar J.W., "A Miniature 500 000-r/min Electrically Driven Turbocompressor", IEEE Transactions on Industry Applications, Vol. 46, n. 6, 2010, pp. 2459-2466.

[6] Bianchi N., Bottesi O., Alberti L., "Energy efficiency improvement adopting synchronous motors" Ecological Vehicles and Renewable Energies (EVER), 2013 8th International Conference and Exhibition on.

[7] http://www.vacuumschmelze.com/

[8] http://www.jfe-steel.co.jp/

[9] Cupertino, F.; Pellegrino, G.; SyR-e User's Manual, Oct. 29 2014, Ver.1.0 [Online]. Available: http://sourceforge.net/projects/syr-e/

[10] Vagati, A.; Pastorelli, M.; Francheschini, G.; Petrache, S.C., "Design of low-torque-ripple synchronous reluctance motors," Industry Applications, IEEE Transactions on , vol.34, no.4, pp.758-765, Jul/Aug 1998.

[11] Cupertino, F.; Pellegrino, G.; Gerada, C., "Design of Synchronous Reluctance Motors With Multi-objective Optimization Algorithms," Industry Applications, IEEE Transactions on , vol.50, no.6, pp.3617,3627, Nov.-Dec. 2014.

[12] Moghaddam, R.R., "High speed operation of electrical machines, a review on technology, benefits and challenges," Energy Conversion Congress and Exposition (ECCE), 2014 IEEE , vol., no., pp.5539,5546, 14-18 Sept. 2014.

[13] Sullivan, C.R.; Zhang, R.Y., "Analytical Model for Effects of Twisting on Litz-Wire Losses", Control and Modeling for Power Electronics (COMPEL), 2014 IEEE 15th Workshop on, 22-25 June 2014.